Journal of Biomolecular NMR, 2 (1992) 335–348
ESCOM

J-Bio NMR 063

Dynamic properties of salmon calcitonin bound to sodium dodecyl sulfate micelles: A restrained molecular dynamics study from NMR data

Maria A. Castiglione Morelli[a,*], Annalisa Pastore[a] and Andrea Motta[b,**]

[a]*European Molecular Biology Laboratory, 6900 Heidelberg, Germany*
[b]*Istituto per la Chimica di Molecole di Interesse Biologico del CNR, 80072 Arco Felice (Napoli), Italy*

Received 20 December 1991
Accepted 24 March 1992

Keywords: Molecular dynamics; Time-averaged distance NMR restraints; Calcitonin; Conformational flexibility; SDS

SUMMARY

We have investigated the conformational behaviour of salmon calcitonin bound to sodium dodecyl sulfate micelles by means of restrained molecular dynamics simulations with both 'static' and time-averaged NMR distance restraints. A more realistic picture of the inherent flexibility of the hormone is obtained when using time averaging. With this approach, long-range NOEs are interpreted better by considering a dynamical exchange among different conformations.

INTRODUCTION

Calcitonin (CT) is a single-chain polypeptide hormone of 32 amino acids. Its best-known action is the inhibition of bone resorption. This is achieved by reducing the plasma levels both of calcium and of inorganic phosphate indirectly via its action on target organs (Austin and Heath, 1981). Structurally, CT is characterized by an amino-terminal disulphide-bridged loop between sites 1 and 7 and a carboxy-terminal proline amide (Scheme 1).

```
1                5                10                15                20
Cys-Ser-Asn-Leu-Ser-Thr-Cys-Val-Leu-Gly-Lys-Leu-Ser-Gln-Glu-Leu-His-Lys-Leu-Gln-Thr-
 |_____________________|
          25                30
Tyr-Pro-Arg-Thr-Asn-Thr-Gly-Ser-Gly-Thr-Pro-NH2
```

Scheme 1. Amino acid sequence of salmon calcitonin.

*Present address: Dipartimento di Chimica, Università della Basilicata, 85100 Potenza, Italy.
**To whom correspondence should be addressed

0925-2738/$ 5.00

Several studies on the structure of calcitonins in different solvent media have been reported (Brewer and Edelhoch, 1970; Epand et al., 1983,1986; Motta et al., 1989,1991a,b; Meyer et al., 1991; Meadows et al., 1991). Calcitonin receptors have been localized mainly on the surfaces of target cells (Breimer et al., 1988) so the interaction of the hormone with the membrane and its conformation in this amphipathic environment are of interest. Within this context, it is recognised that micelles are an acceptable model to mimic the membrane environment (Brown, 1979; Gierasch et al., 1982). For example, the interactions in the sodium dodecyl sulfate (SDS) micelles are representative of those important for protein–lipid associations in the membrane (Gierasch et al., 1982). The study of calcitonin in micelles can therefore be considered a useful approximation to its membrane-bound form. For this reason, we have studied the conformation of salmon calcitonin (sCT) bound to SDS micelles using 2D NMR, distance geometry (DG) calculations and restrained energy minimization (rEM) (Motta et al., 1991b).

We found that the structure of sCT is helical between residues 6 and 22, with two less well defined terminal regions. The C terminus folds back towards the helix. It became clear while refining the structure that the long-range distance restraints could not all be satisfied simultaneously, which might be explained by the existence of dynamically interchanging conformations. This situation seemed to be an ideal example for applying the recently proposed time-averaged restrained molecular dynamics (rMD) (Torda et al., 1990), which incorporates time-averaged information explicitly.

We present here, therefore, a molecular dynamical investigation into the conformational flexibility of sCT, comparing the results obtained by both 'conventional' and time-averaged rMD. The results are compared with experimental NMR data on NOE target distances, coupling constants and amide exchange rates.

METHODS

Analysis of the NOESY data produced 260 interproton distance restraints that were used as input for the DG calculations (Motta et al., 1991b). Twelve out of 23 β-methylene groups were stereospecifically assigned with the program HABAS (Güntert et al., 1989). The procedure suggested by Esposito et al. (1987) was used for Gly^{10}. Initial structures were generated using the program DIANA (Güntert et al., 1991) and the best structures (in terms of the target function values) were subjected to rEM as described before (Motta et al., 1991b).

Five structures were then selected for rMD calculations. All EM and MD calculations were performed with the GROMOS software package (van Gunsteren and Berendsen, 1987). Bond-length constraints were applied with the SHAKE algorithm (van Gunsteren and Berendsen, 1977; Ryckaert et al., 1977). The rMD time step was 2 fs.

Initial velocities were taken from a Maxwellian distribution appropriate for the two starting temperatures, 300 K and 900 K. The temperatures were stabilised by coupling to a thermal bath during the MD runs (Berendsen et al., 1984). In the simulations at 300 K we used a coupling time constant of 0.01 ps during the first ps of the equilibration period and 0.1 ps thereafter. In the simulation at 900 K a time constant of 0.01 ps was used for the first 11 ps. This was followed by 10 ps of cooling to 300 K, with a time constant of 2 ps, and a time constant of 0.1 ps was used in the successive 40 ps of the simulation.

The list of nonbonded neighbouring atom pairs was updated every 10 cycles of the EM and eve-

ry 10 steps of 2 fs during the MD. A cut-off radius of 0.8 nm was used, beyond which no non-bonded interactions were evaluated. Distance restraints obtained from NMR measurements were incorporated in the calculations as a semiharmonic potential function with a force constant of 1000 kJ nm^{-2} mol^{-1} during the dynamics and the final energy minimization.

In the MD simulation at 900 K a force constant of 4000 kJ nm^{-2} mol^{-1} was used during the first 11 ps, reduced thereafter to 1000 kJ nm^{-2} mol^{-1}.

Time-averaged distance restraint simulations (Torda et al., 1990) were performed at 300 K, after an initial picosecond of standard MD. According to Torda et al. (1990), the weighting function used for averaging was:

$$\bar{r}(t) = \int_0^t \{(1/\tau)\exp(-t'/\tau)\,[r(t-t')]^{-3}\,dt'\}^{-1/3}$$

where τ is the exponential decay constant. The τ values used in calculating the running average in time-averaged distance restraints should be large enough to allow for the necessary conformational changes to occur. It was estimated that in order to achieve reasonable averaging, the length of the trajectory should be approximately an order of magnitude larger than τ (Torda et al., 1989). The time constants for the memory function were 0, 4 and 8 ps, and the force constants were 1000 and 2500 kJ nm^{-2} mol^{-1}. The initial values of the time-averaged distances were obtained by subtracting 0.02 nm from the distances calculated from the measured NOEs. In one of the trajecto-

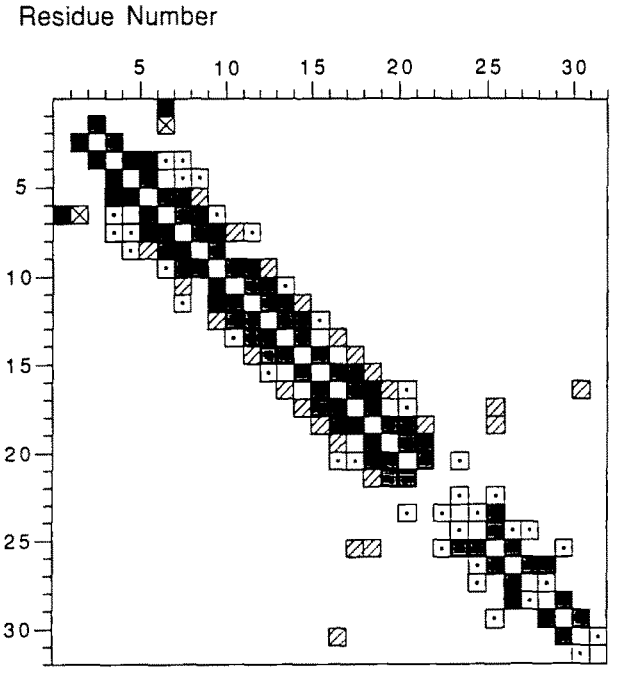

Fig. 1. Survey of sequential and long-range NOE-derived distance restraints for sCT bound to SDS micelles. Both axes represent the amino acid sequence. Filled squares at position (x,y) indicate that a NOE between backbone amide protons of the two residues in the sequence locations x and y was observed, while a dotted square indicates a CαH NH-type NOE. A shaded square indicates a NOE between NH or CαH of one residue and a side-chain proton in another residue. The square containing a cross indicates a NOE between side-chain protons of the two residues.

ries, the initial value of one of the distances (namely, Lys^{18} to Asn^{26}) was set 0.26 nm longer to increase its relative weight. The time constant for coupling to the temperature bath was 0.04 ps during the whole simulation. These simulations were 80 ps long but only the final 40 ps were used for averaging and analysis.

Two hundred steps of conjugate-gradient rEM were performed on the final time-averaged structures.

All simulations were performed in vacuo.

The hydrogen-bond criteria used in the analysis were that hydrogen bonds could be formed if the distances hydrogen–acceptor were equal to or lower than 0.25 nm and if the angles donor–hydrogen–acceptor were equal to or larger than 135°.

Graphical representation was carried out with the interactive graphics program WHATIF (Vriend, 1990) running on an Evans and Sutherland PS390 graphics system. All calculations were carried out on the Local Area Vax Cluster of the European Molecular Biology Laboratory at Heidelberg (Germany).

RESULTS AND DISCUSSION

Figure 1 shows a diagonal plot of the experimental NOE data which were used as input distance restraints in the DG calculations (Motta et al., 1991b). NOEs observed at different mixing times (60, 120 and 200 ms) are represented by squares linking the residues involved. Almost all of them can be classified as short- and medium-range effects apart from three long-range NOEs: Thr^{31}NH-$His^{17}CH_2\beta$, Asn^{26}NH-$Lys^{18}CH_2\delta$ and Asn^{26}NH-$Leu^{19}CH\gamma$. They were positively identified and all detected at 60-ms mixing time. Their intensities were greater at 120- and 200-ms mixing times. Recently, Fejzo et al. (1991) discussed the effects on the determination of protein solution structures caused by hybrid exchange mechanisms which have the potential of transferring cross relaxation over long distances. In their example, long-range spin-diffusion artefacts were mediated by chemical exchange processes. However, in spite of the putative mobility of the sCT molecule, we were not able to identify any chemical exchange process under our experimental conditions which may have caused errors in the estimation of distances.

The conformational space of SDS-bound sCT consistent with the above experimental NMR data was explored by performing rMD simulations on some of the previously determined DG structures (Motta et al., 1991b). The five best structures (in terms of energy values and distance restraint violations) were then selected and indifferently used for the rMD simulations performed as described below.

'Conventional' rMD simulations

For three of the selected structures, an 80-ps long simulation (referred to as sCT1 in Table 1) and two 60-ps long simulations (sCT2 and sCT3 in Table 1) were carried out at 300 K. The last 40 ps were used for calculating time averages of various properties and for obtaining an average structure. Table 1 briefly describes the resulting structures.

The main effect of rMD refinement is to lower the energy of the system because the method is able to overcome local energy barriers and to reliably locate the region's global minimum (Clore and Gronenborn, 1987). The potential energies of the time-averaged energy-minimized structures were, indeed, all in a relatively narrow range (-1972 to -2098 kJ mol^{-1}).

TABLE 1
PROPERTIES OF sCT STRUCTURES RESULTING FROM rMD

Structure[a]	Energies (kJ mol^{-1})[b]				$\Sigma_{violation}$[c] (nm)	Average restraint violation[d] (nm)	Number violations >0.1 nm[d]
	Pot	vdW	El	Dist rest			
sCT1	−2098	−957	−1606	66	1.90	0.01	1(0.20)
sCT2	−1972	−970	−1571	128	2.61	0.01	1(0.58)
sCT3	−2017	−1034	−1601	111	2.66	0.03	2(0.40)
sCT_{900}	−2080	−967	−1586	71	2.13	0.02	1(0.24)
sCT_{aver0}	−2103	−977	−1594	72	1.83	0.01	2(0.26)
sCT_{aver1}	−2056	−987	−1576	81	2.23	0.01	1(0.18)
sCT_{aver2}	−1738	−928	−1610	64	1.86	0.01	1(0.13)
sCT_{aver3}	−2022	−959	−1630	81	2.41	0.01	3(0.22)
sCT_{aver4}	−1765	−957	−1660	84	2.60	0.01	1(0.19)

[a] sCT1, structure obtained after 80 ps of rMD simulation at 300 K; sCT2, sCT3, structures obtained after 60 ps of rMD simulation at 300 K; sCT_{900}, structure obtained after 60 ps of rMD simulation at 900 K; sCT_{aver0}, sCT_{aver1}, sCT_{aver2}, sCT_{aver3}, sCT_{aver4}, structures obtained after 80 ps of rMD at 300 K with time-averaged distance restraints and, respectively, with time constants for the memory function of 0 ps (sCT_{aver0}), 4 ps (sCT_{aver1}, sCT_{aver2}) and 8 ps (sCT_{aver3}, sCT_{aver4}) and force constants of 1000 (sCT_{aver0}, sCT_{aver1}, sCT_{aver3} and sCT_{aver4}) and 2500 kJ nm^{-2} mol^{-1} (sCT_{aver2}). For sCT_{aver4} an additional correction of 0.26 nm was applied to the distance 18–26.

[b] Energy data are relative to the energy-minimized structures averaged over the last 40 ps of the MD simulations. Pot, total potential energy; vdW, van der Waals steric nonbonded energy; El, electrostatic nonbonded energy; Dist rest, energy associated with NOE distance restraints.

[c] Data are relative to average values calculated over the last 40 ps of MD trajectory.

[d] Numbers in parentheses indicate maximum distance violations.

Figure 2 shows a superposition of four snapshots of sCT generated in the time range 50–80 ps of the MD simulation, with equal time intervals of 10 ps (namely simulation sCT1 of Table 1). Residues 6 to 22 form a well-defined helix, while the N terminus and especially the C terminus do not converge to a unique structure because of the fewer NOE data. However, interresidual NOEs and backbone torsion angles justify the inclusion of Thr^{6} and Cys^{7} into the helix (Motta et al., 1991b). On the contrary, although the φ and ψ angles for Leu^{4} are in the allowed α-helical region, the lack of convergence among the structures for Ser^{5} does not warrant the inclusion of residues 4 and 5 into the helix (Motta et al., 1991b). The 6-22 central helix is rather rigid but the rest of the molecule is more flexible. This picture is confirmed by the observation of the RMS fluctuations of the φ and ψ angles for the rMD runs (data not shown). Indeed, the N and the C termini exhibit the largest variations of the dihedral angles.

The sums of violations calculated in the trajectories are reported in Table 1, together with the average relative restraint violations. The latter values are low in all structures; however, there is always a restraint violation in excess of 0.2 nm in each structure corresponding to the observed long-range NOE between the NH of Asn^{26} and the δ protons of Lys^{18}. The simultaneous fulfillment of this restraint and the other long-range NOE between the NH of Asn^{26} and the γ proton of Leu^{19} seems to be impossible. For these cross peaks upper limits of 0.65 nm and 0.50 nm were assigned, respectively. The fluctuation of the system amongst several conformations could be the

explanation of these consistently high violations. The system must spend a fraction of time in conformations which satisfy only one of the two distances but never both simultaneously. This can be observed in a plot of the NOE violations as a function of their sizes taken at different snapshots of the trajectories. Figure 3 shows the number of distance restraint violations for structure sCT1 during the time span of 60–80 ps. The NOE between the NH of Asn^{26} and the δ protons of Lys^{18} is always the largest violation at all times (including 50 ps, data not shown) but at 70 ps (Fig. 3B) the size of the violation is consistently lower. This indicates that at this time of the simulation the conformation of the molecule conforms better with the experimental distance restraints.

In order to take advantage of the effect of increased temperature in overcoming local energy barriers and of possibly locating different global minima, we performed simulated-annealing calculations on the fourth of the selected structures using a temperature of 900 K during the first 11 ps followed by another 50 ps at 300 K. The last 40 ps were then used for averaging and analysis (simulation sCT_{900} in Table 1). The time-averaged energy-minimized structure had a potential energy of -2080 kJ mol^{-1} and a distance restraint energy of 71 kJ mol^{-1}. No significant structu-

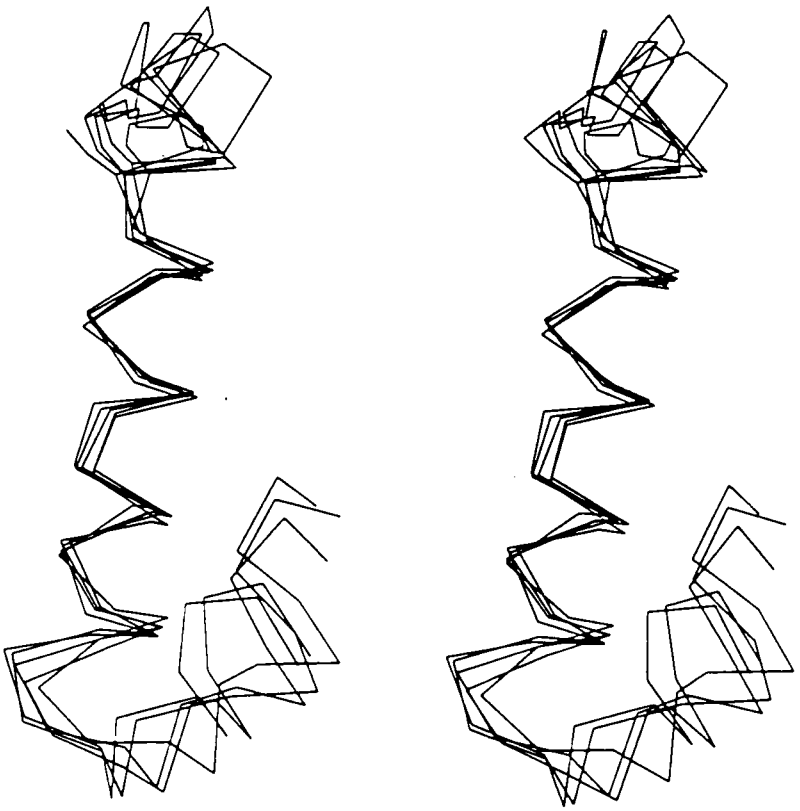

Fig. 2. Superposition of the Cα atoms of the structures of sCT (simulation sCT1 in Table 1) generated in the range 50–80 ps with a 10-ps time interval. Structures were superimposed for pairwise minimum RMSD of the Cα atoms of residues 6–22 with the time-averaged energy-minimized structure.

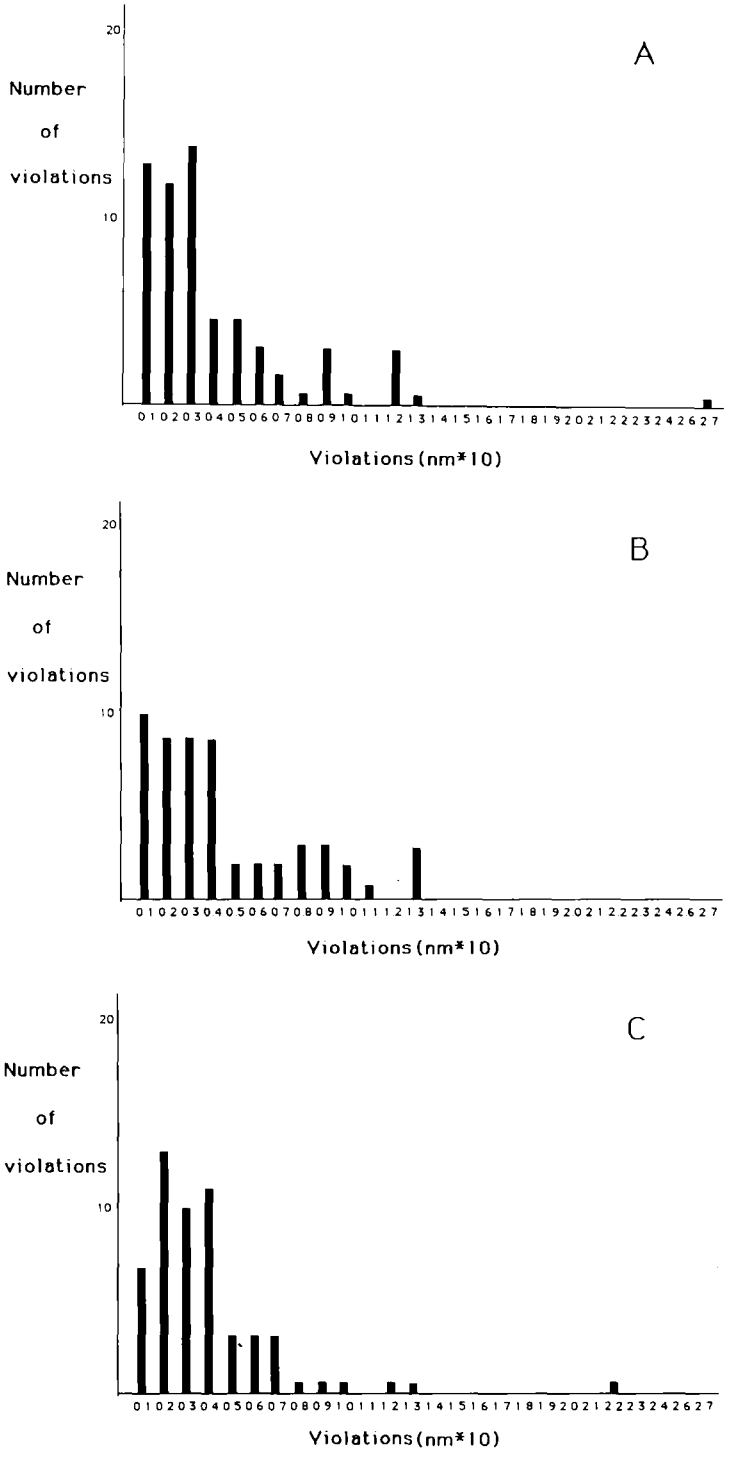

Fig. 3. Number of distance-restraint violations as a function of their size (nm). Data are reported for the time period 60-80 ps of the rMD simulation on structure sCT1. (A) 60 ps; (B) 70 ps; (C) 80 ps.

ral shifts were observed with the changing simulation temperature. The largest violation of the distance between the NH of Asn^{26} and the δ protons of Lys^{18} was observed in this simulation.

The possibility that long-range NOEs stemmed from different structures simultaneously present in solution was also investigated. The following approach was used to obtain a rough characterization of the conformations present and their mutual compatibility. Two hundred cycles of energy minimization including arbitrary pairs of the three long-range restraints in addition to the whole list of short- and medium-range NOEs were performed. The results showed that, while the 19–26 and the 17–31 NOEs are mutually compatible, a large violation was always present when including the 18–26 distance. Two simulated-annealing runs of 10 ps, at 500 K and with a force constant of 4000 kJ nm^{-2} mol^{-1}, were calculated including the two sets of incompatible restraints separately and the results were minimized. Figure 4 depicts the ribbon representation of the two

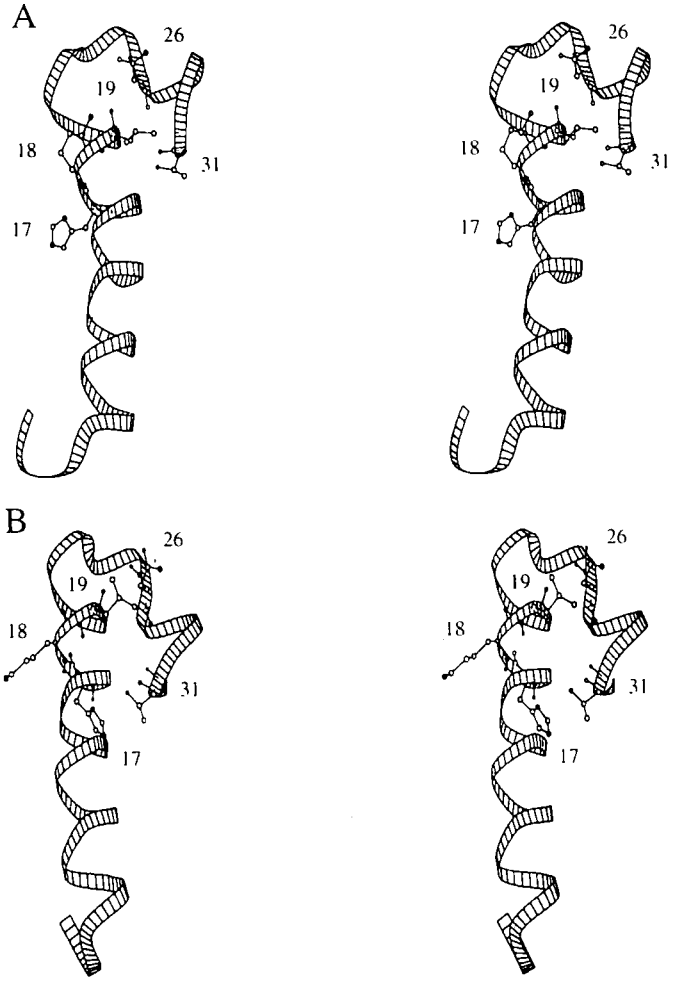

Fig. 4. Stereoview of two limiting structures of sCT obtained including in the long-range distance restraint list (A) only the 18–26 distance, and (B) only the 19–26 and the 17–31 distances. For clarity, the backbone is represented as a ribbon with the side chain of the residues involved in long-range NOEs explicitly shown.

limiting structures, with the side chains of the residues involved in the long-range NOEs explicitly drawn. The resulting two limiting structures are almost isoenergetic ($E_{pot} = -1971$ kJ mol^{-1} and $E_{dist\ rest} = 48$ kJ mol^{-1} for the structure including only the 18–26 restraint (Fig. 4A), and $E_{pot} = -2049$ kJ mol^{-1} and $E_{dist\ rest} = 37$ kJ mol^{-1} for the other structure). The main differences are the orientation of the C-terminal loop and the rearrangement of some of its side chains. However, since this approach relies on an arbitrary choice of compatible long-distance pairs, it does not allow an objective characterization of the possible structures. This makes the structures in Fig. 4 unreal and suggests that the flexibility of the system has to be accounted for to justify the simultaneous presence of the long-range NOEs.

Hydrogen bonds. Hydrogen bonds, previously incluced for the helical region, in the DG calculations, were switched off during MD simulations to check their consistency. Table 2 reports calculated hydrogen-bond occupancies for sCT as obtained from different rMD trajectories. A good agreement is obtained with the experimentally observed slowly exchanging protons. In most of the trajectories, the N-terminal ring is stabilized by an H bond between the NH of Thr^{6} and the O$^{\delta 1}$ of Asn^{3} with a high percentage of occurrence; few other H bonds are also present, though not in all simulations and not with a high occupancy. A hydrogen bond between the CO of Pro^{23} and the NH of Thr^{25} (simulations sCT1, sCT$_{900}$) or the NH of Asn^{26} (simulations sCT2, sCT3) indicates a bend of the molecule at the end of the helical region. Few long-range H bonds — namely OH$^{\gamma}$ of Ser^{13}–O$^{\gamma}$ of Thr^{31} (sCT1), OH$^{\varepsilon 1}$ of Glu^{15}–O^{1} of Pro^{32} (sCT3), NH of Gly^{30}–CO of Arg^{24} (sCT3), OH$^{\gamma}$ of Thr^{31}–O$^{\varepsilon 1}$ of Gln^{20} (sCT2, sCT$_{900}$) and NH of Thr^{31}–CO of Leu^{16} (sCT1) — stabilize the folding of the hormonal tail toward the helix 6–22, as already found in the DG structures (Motta et al., 1991b). The presence in all simulations of an H bond between the NH of Thr^{27} and the CO of Arg^{24} further characterizes this part of the molecule. The conformational freedom associated with the terminal region of the peptide might be related to the ability of forming dynamically different hydrogen bonds.

J coupling constants. $J_{NHC\alpha H}$ coupling constants averaged over the different trajectories show the best convergence among different trajectories from residues 4 to 18 (data not shown). Outside this range, a larger scattering of J values together with a poorer agreement with the experimental data is observed. Longer MD simulations would certainly help to obtain a better sampling of the multiple conformations contributing to the observed values.

Time-averaged distance restraints

For small molecules existing in solution in equilibrium between two different conformations it is not possible to satisfy all the experimental restraints simultaneously by conventional rMD because this would be equivalent to trying to generate some physically unrealistic single conformation (Torda et al., 1990). With larger molecules, however, it may not be possible to identify the distinct conformational states among which the molecules move, because measured NOEs are only average values reflecting the whole configurational space visited by the molecules on the NMR time scale.

Time-averaged rMD has been recently suggested as a more efficient method for structure refinement (Torda and van Gunsteren, 1991). Applications to NMR data have been presented for Tendamistat (Torda et al., 1990) and in a model study of DNA (Pearlman and Kollman, 1991). According to this approach, the molecule is not forced to satisfy distance restraints at each time point of the simulation but only on average over the course of the trajectory (Torda et al., 1989).

TABLE 2
CALCULATED HYROGEN-BOND OCCUPANCIES (%) FROM rMD TRAJECTORIES

Donor	Acceptor	Trajectories[a]				H Bonds[b]
		sCT1	sCT2	sCT3	sCT_{900}	
NH Ser^{2}	O^{γ} Thr^{6}	70				
OH^{γ} Ser^{2}	$O^{\delta 1}$ Asn^{3}		55			
NH Asn^{3}	O^{γ} Thr^{6}	64				
NH Thr^{6}	$O^{\delta 1}$ Asn^{3}	84		66	76	*
NH Cys^{7}	O Asn^{3}	97	92	96	99	
NH Val^{8}	O Leu^{4}	89	92	93	96	*
NH Leu^{9}	O Ser^{5}	100	98	100	100	*
NH Gly^{10}	O Thr^{6}	85	85	87	91	*
NH Lys^{11}	O Cys^{7}	94	89	93	92	*
NH Leu^{12}	O Val^{8}	100	99	99	100	*
NH Ser^{13}	O Leu^{9}	94	86	99	95	*
OH^{γ} Ser^{13}	O Leu^{9}	63				
OH^{γ} Ser^{13}	O^{γ} Thr^{31}	54				
NH Gln^{14}	O Gly^{10}	98	95	97	89	*
NH Glu^{15}	O Lys^{11}	94	95	97	96	*
$OH^{\epsilon 1}$ Glu^{15}	O^{1} Pro^{32}			52		
$OH^{\epsilon 1}$ Glu^{15}	O Gln^{14}		59			
NH Leu^{16}	O Leu^{12}	98	96	99	99	*
NH His^{17}	O Ser^{13}	95	99	96	99	*
$N^{\delta 1}$ His^{17}	$O^{\epsilon 1}$ Gln^{14}				75	
$N^{\delta 1}$ His^{17}	$O^{\epsilon 1}$ Gln^{20}	68	61	61		
N^{ζ} Lys^{18}	O Glu^{15}			51		
NH Lys^{18}	O Gln^{14}	91	95	97	95	*
NH Leu^{19}	O Glu^{15}	96	96	97	96	*
NH Gln^{20}	O Leu^{16}	97	92	47	90	*
NH Thr^{21}	O Lys^{18}		61	42	54	
OH^{γ} Thr^{21}	O His^{17}	68	63			
NH Thr^{21}	O His^{17}	66	34	61	44	*
NH Tyr^{22}	O Lys^{18}	68	89	89	68	*
NH Arg^{24}	O Thr^{21}	51			92	*
N^{ζ} Arg^{24}	O Tyr^{22}			60		
OH^{γ} Thr^{25}	$O^{\delta 1}$ Asn^{26}			67	48	
NH Thr^{25}	O Pro^{23}	87			92	
NH Asn^{26}	O Pro^{23}		90	99		
$N^{\delta 1}$ Asn^{26}	O^{γ} Ser^{29}		62		72	
NH Thr^{27}	O Arg^{24}	73	42	92	79	
OH^{γ} Thr^{27}	O Arg^{24}			71		
OH^{γ} Thr^{27}	O Gly^{30}			54		
NH Gly^{28}	O Thr^{25}			62	49	
NH Ser^{29}	O Thr^{27}		79			
OH^{γ} Ser^{29}	O Gly^{28}		87			
NH Gly^{30}	O Arg^{24}			83		
NH Gly^{30}	O Asn^{26}				64	
NH Thr^{31}	O Leu^{16}	46				
OH^{ζ} Thr^{31}	$O^{\epsilon 1}$ Gln^{20}		45		83	
NH Thr^{31}	O Thr^{27}				83	
NH Thr^{31}	O Gly^{28}				57	

[a] The same notation of Table 1 was used for the structures to identify the trajectories: sCT1, trajectory over 80 ps; sCT2, sCT3, trajectories over 60 ps; sCT_{900}, trajectory simulated at 900 K over 60 ps.

[b] Hydrogen bonds experimentally identified through exchange experiments. Amides with slow exchange rates were present during the $^{2}H_{2}O$ exchange NOESY experiment which lasted 24 h (pH 3.3, T = 310 K). Amide protons with fast exchange rates had no detectable resonance intensity in this type of experiment.

The method is therefore particularly suitable to describe the behaviour of molecules which exist as a dynamic envelope of conformations.

A time-dependent distance-restraint approach, with different values of the memory function time constant, was applied to sCT to allow more mobility and improve the agreement with the experimental distance restraints. The presence of the three long-range NOEs should hopefully be accounted for, with a corresponding lowering of the size of the violations. 80-ps long simulations were performed using the fifth of the selected structures as the starting conformation. Only the last 40 ps were used for analysis (simulations sCT_{aver} in Table 1). The sum of violations and the size of the largest violations are smaller than those obtained without the application of time-averaged NOEs (compare with sCT_{aver0} which corresponds to an rMD simulation without time averaging on the same starting structure). In this respect, the best results were obtained using a memory function time constant of 4 ps and a force constant of 2500 kJ nm^{-2} mol^{-1} (sCT_{aver2} in Table 1), although the use of a larger force constant value reduces the distance violations at the expense of intramolecular energy, leading to a more strained structure (van Gunsteren and Berendsen, 1990). The relative degree of mobility for different regions of the sCT molecule is evi-

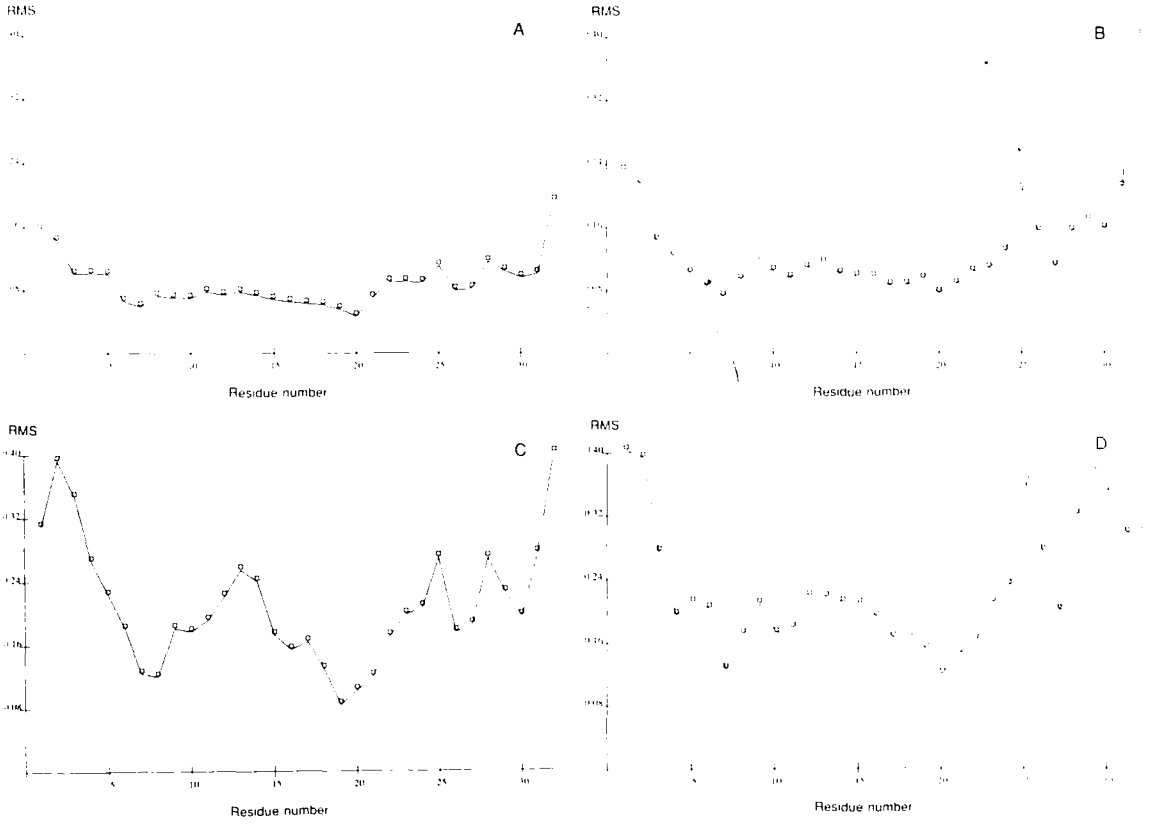

Fig. 5. RMS fluctuations (nm) of the Cα position for each sCT residue as derived from an 80-ps rMD trajectory with time-averaged distance restraints. Data are averaged from the last 40 ps of trajectories. (A) no memory, K_{dc} = 1000 kJ nm^{-2} mol^{-1}; (B) τ_{memory} = 4 ps, K_{dc} = 1000 kJ nm^{-2} mol^{-1}; (C) τ_{memory} = 4 ps, K_{dc} = 2500 kJ nm^{-2} mol^{-1}; (D) τ_{memory} = 8 ps, K_{dc} = 1000 kJ nm^{-2} mol^{-1}.

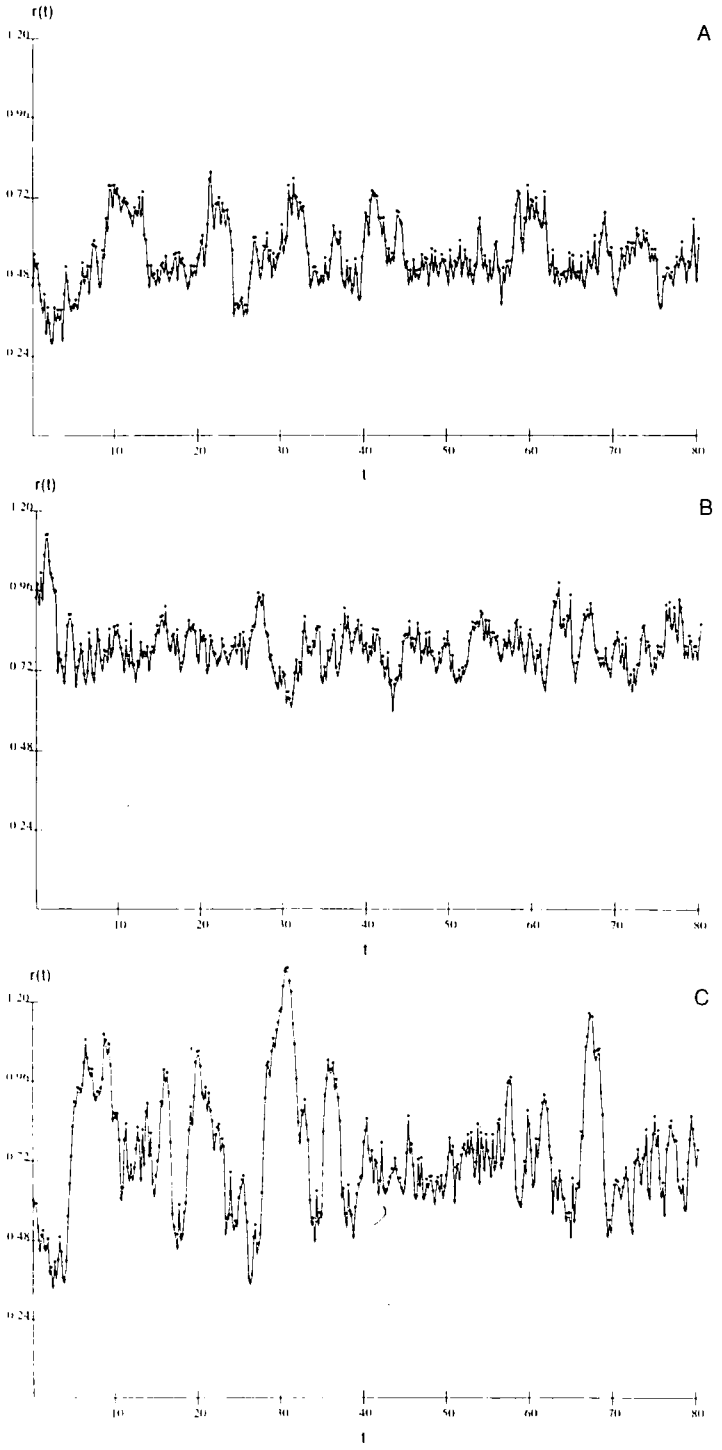

Fig. 6. Interatomic distances (nm) as a function of time (ps) during 80 ps of MD simulation using time-averaged distance restraints (time constant of the memory function = 4 ps). (A) distance between the NH of Asn^{26} and the γ proton of Leu^{19}; (B) distance between the NH of Asn^{26} and the δ protons of Lys^{18}; (C) distance between the NH of Thr^{31} and the β protons of His^{17}. The distance restraints for A, B, C are 0.50, 0.65 and 0.65 nm, respectively.

dent in the RMS fluctuations of the Cα atom positions as derived from rMD trajectories (see Fig. 5). This provides some measure of the conformational space spanned during the trajectories. The mobility of the N- and C-terminal regions of the molecule is strongly enhanced. The largest fluctuations were observed when increasing the distance-restraint force constant. This results in a larger driving force to move among different conformations (Figs. 5B and C).

In addition to a general increase of the overall mobility, differential behaviour of specific regions of the molecule may be observed by plotting the dependence of distances as a function of time during the simulation. Figure 6 shows the behaviour of the distances between the NH of Asn^{26} and the γ proton of Leu^{19}, the NH of Asn^{26} and the δ protons of Lys^{18} and the NH of Thr^{31} and the β protons of His^{17}. It can be seen that these distances show large fluctuations and that the NOE bonds are violated for many picoseconds during the trajectory. However, when using time-averaged distance restraints the experimental NOE data are, on average, better reproduced. The three long-range distances involve residues far apart in the sequence and therefore reflect internal motions and the interplay of many NOE restraints. This situation resembles the mobility observed for Tyr^{15} in Tendamistat which alternately satisfies the NOEs to residues 13 and 17, although in this example the residues involved are closer in the polypeptide sequence (Torda et al., 1990).

One of the trajectories was performed with an initial value for the distance 18–26 adding 0.26 nm to the distance calculated from the measured NOE, which corresponds to an increased weight of the above distance. A memory of 8 ps was used (sCT_{aver4} in Table 1). No significant changes in the trajectories were observed and the dependence of this distance vs. time differs only in the first picosecond from the behaviour shown in Fig. 6B (data not shown). The energy of the resulting structure sCT_{aver4} is higher in comparison to that of structure sCT_{aver3} obtained with the same memory-function time constant. The increased weight given to the 18–26 distance alone is not sufficient to restrain the system: the time constant is too long and the system mobility increases. Once the system has reached the desired conformation, energetic terms hinder motion away from that conformation (Torda et al., 1989).

The time scale of an MD simulation for an isolated molecule is faster than the real behaviour in solution, so in reality the process does not happen with the same frequency and fluctuations may be smaller. However, the results of this simulation suggest that the NH of Asn^{26} for some time is near to the δ protons of Lys^{18} and for some other time is near to the γ proton of Leu^{19}. The constant violation in all simulations of one or more of these observed short restraints to distant sites of the molecule might be invoked as the type of artefact expected from averaging of NOEs over two or more discrete structures (Kim and Prestegard, 1989).

CONCLUSIONS

sCT in a micelle environment provides an interesting example of dynamically exchanging multiple conformations. Our interest in the dynamic properties of sCT is motivated by the possible implications of the conformational flexibility for the biological activity of the hormone and its folding process. We have discussed here ways to describe the dynamical properties of this system by comparing results both from static and time-averaged rMD. As expected, the latter method produced better agreement with experimental distance bounds, increased the allowed molecular mobility and gave a more realistic estimate of possible conformations occupied by the hormone in solution.

ACKNOWLEDGEMENTS

We would like to thank Dr. A.E. Torda for useful discussions and the use of his programs on time-averaged distance restraints, Dr. F. Fraternali for helpful discussions, Dr. G. Vriend for his kind assistance in using WHATIF, Dr. N.A. Goud for the sample of calcitonin, Prof. A.M. Lesk for the use of his program for Fig. 4, and Dr. D.J. Thomas for critical reading of the manuscript.

REFERENCES

Austin, L.A. and Heath, H. (1981) *N. Engl. J. Med.*, **304**, 269–278.
Berendsen, H.J.C., Postma, J.P.M., van Gunsteren, W.F., Di Nola, A. and Haak, J.M. (1984) *J. Chem. Phys.*, **81**, 3684–3690.
Breimer, L.H., MacIntyre, I. and Zaidi, M. (1988) *Biochem. J.*, **255**, 377–390.
Brewer, H.B. and Edelhoch, H. (1970) *J. Biol. Chem.*, **245**, 2402–2408.
Brown, L.R. (1979) *Biochim. Biophys. Acta*, **577**, 135–148.
Clore, G.M. and Gronenborn, A.M. (1987) *Prot. Eng.*, **1**, 275–288.
Epand, R.M., Epand, R.F., Orlowski, R.C., Schlueter, R.J., Boni, L.T. and Hui, S.W. (1983) *Biochemistry*, **22**, 5074–5084.
Epand, R.M., Epand, R.F., Orlowski, R.C., Seyler, J.K. and Colescott, R.L. (1986) *Biochemistry*, **25**, 1964–1968.
Esposito, G., Carver, J.A., Boyd, J. and Campbell, I.D. (1987) *Biochemistry*, **26**, 1043–1050.
Fejzo, J., Krezel, A.M., Westler, W.M., Macura, S. and Markley, J.L. (1991) *Biochemistry*, **30**, 3807–3811.
Gierasch, L.M., Lacy, J.E., Thompson, K.F., Rockwell, A.L. and Watnick, P.I. (1982) *Biophys. J.*, **37**, 275–284.
Güntert, P., Braun, W., Billeter, M. and Wüthrich, K. (1989) *J. Am. Chem. Soc.*, **111**, 3997–4004.
Güntert, P., Braun, W. and Wüthrich, K. (1991) *J. Mol. Biol.*, **217**, 517–530.
Kim, Y. and Prestegard, J.H. (1989) *Biochemistry*, **28**, 8792–8797.
Meadows, R.P., Nikonowicz, E.P., Jones, C.R., Bastian, J.W. and Gorenstein, D.G. (1991) *Biochemistry*, **30**, 1247–1254.
Meyer, J.-P., Pelton, J.T., Hoflack, J. and Saudek, V. (1991) *Biopolymers*, **31**, 233–241.
Motta, A., Castiglione Morelli, M.A., Goud, N.A. and Temussi, P.A. (1989) *Biochemistry*, **28**, 7998–8002.
Motta, A., Temussi, P.A., Wünsch, E. and Bovermann, G. (1991a) *Biochemistry*, **30**, 2364–2371.
Motta, A., Pastore, A., Goud, N.A. and Castiglione Morelli, M.A. (1991b) *Biochemistry*, **30**, 10444–10450.
Pearlman, D.A. and Kollman, P.A. (1991) *J. Mol. Biol.*, **220**, 457–479.
Ryckaert, J.P., Ciccotti, G. and Berendsen, H.J.C. (1977) *J. Comp. Phys.*, **23**, 327–341.
Torda, A.E., Scheek, R.M. and van Gunsteren, W.F. (1989) *Chem. Phys. Lett.*, **157**, 289–294.
Torda, A.E., Scheek, R.M. and van Gunsteren, W.F. (1990) *J. Mol. Biol.*, **214**, 223–235.
Torda, A.E. and van Gunsteren, W.F. (1991) *Comp. Phys. Commun.*, **62**, 289–296.
van Gunsteren, W.F. and Berendsen, H.J.C. (1977) *Mol. Phys.*, **34**, 1311–1327.
van Gunsteren, W.F. and Berendsen, H.J.C. (1987) *Groningen Molecular Simulation (GROMOS) Library Manual*, BIOMOS, Groningen, The Netherlands, pp. 1–229.
van Gunsteren, W.F. and Berendsen, H.J.C. (1990) *Angew. Chem. Int. Ed. Engl.*, **29**, 992–1023.
Vriend, G. (1990) *J. Mol. Graphics*, **8**, 52–56.